FEDSM-ICNMM2010-30450

A HIGH-ORDER LES TURBULENT MODEL TO STUDY UNSTEADY FLOW CHARACTERISTICS IN A LOW PRESSURE TURBINE CASCADE

Tomohiko Jimbo   **Debasish Biswas**

Corporate Research and Development Center
TOSHIBA Corporation
1, Komukai Toshiba-cho, Saiwai-ku, Kawasaki, 212-8582, Japan

ABSTRACT

In this work, unsteady viscous flow analysis around Low Pressure Turbine (LPT) cascade using a High-Order LES (Large Eddy Simulation) turbulence model is carried out to investigate basic physical process. In the aerospace industry, input shaft power for fan and compressor components of turbine engines is most commonly supplied by the LPT. Considering this fact, in the endeavor of developing engines of increased efficiency and decreased weight LPT is an important component worth paying attention. Therefore, a better understanding of low-Reynolds number flow transition and separation behavior is very much essential to such improvements. Blades in the LPT environment may be designed for higher loading if the effects of passing wakes on bypass transition are properly included in the design. Also, under the LPT working conditions, boundary layers along a large extent of blade surface can remain laminar, even in the presence of elevated free-stream turbulence levels. The laminar boundary layers are then particularly susceptible to flow separation over the aft portion of blade suction surfaces, causing blockage in flow passages and a significant reduction in turbine efficiency. Related to weight reduction, the blade spacing in LPT can be increased with a rise in per blade loading. Increased blade spacing however, is accompanied by more extensive boundary layer separation on the suction surface of each blade due to uncovered turning, resulting in a further reduction of efficiency and additional wake losses. In the present work, experimental work is numerically simulated. Features of the flow-fields are described and compared with the experimental data on baseline case and active flow separation control using Vortex Generator Jet (VGJ).

1   NOMENCLATURE

$C_k, C_\varepsilon, \sigma_k$: model parameter
ν, ν_t : viscosity, sub-grid scale viscosity
k_{sgs} : SGS turbulent kinetic energy
L_{ij} : sub-test scale Leonard's stress
S_{ij} : rate of strain tensor
Δ : filter width
τ_{ij} : SGS shear stress
τ_{sgs} : sub-grid scale turbulent time scale
x, y, z : cartesian coordinates
u, v, w : cartesian velocity component in the x, y, z directions
$\overline{}$: grid filter
$\sim$: test filter

2   INTRODUCTION

In the aerospace industry, input shaft power for fan and compressor components of turbine engines is most commonly supplied by the Low Pressure Turbine (LPT). Considering this fact, in the endeavor of developing engines of increased efficiency and decreased weight LPT is an important component worth paying attention. Therefore, a better understanding of low-Reynolds number flow transition and separation behavior is very much essential to such improvements. Blades in the LPT environment may be designed for higher loading if the effects of passing wakes and elevated turbulence on bypass transition are properly included in the design. Also, under the LPT working conditions, boundary layers along a large extent of blade surface can remain laminar, even in the presence of elevated free-stream turbulence levels. The laminar boundary layers are then particularly susceptible to flow separation over the aft portion of blade suction surfaces, causing blockage in flow passages and a significant reduction in turbine efficiency. Related to weight reduction, the blade spacing in LPT can be increased with a rise in per blade loading. Increased blade spacing however, is accompanied by more extensive boundary layer separation on the suction surface of each blade due to uncovered turning, resulting in a further reduction of efficiency and additional wake losses. Recently, active flow control in the form of both steady and pulsed Vortex Generator Jet (VGJ) is one of the techniques to avoid such massive separation occurred on the suction surface of each blade due to uncovered turning. The major effect of flow control using this technique is to increase fullness of the profiles through momentum transfer from the jet and mixing with the boundary layer. In the present work, experimental work of Sondergaard [1] is numerically simulated. Control of the highly-loaded LPT flow separation considered by Sondergaard consisted of steady vortex generator. Recently Computational Fluid Dynamics (CFD) started

playing an important role in the design and development of turbo-machines. Over the last two decades steady progress has been made in the development of CFD for turbo-machinery blade rows [2]-[9]. The eventual goal of these analyses is time accurate model of 3-D flow through blade rows. In general in the numerical study of flow behavior in LPT, Reynolds Averaged Navier-Stokes (RANS) equations are solved [10]-[14]. However, because of the limitations and shortcoming of RANS turbulence models in describing accurately the low-Reynolds separation and the transition to turbulent flow phenomena, these efforts have only been partially successful in predicting some of the overall features of the turbo-machinery flow fields. Moreover, because of several deficiencies in physics-based turbulence modeling based on the RANS approach, this is expected to be inadequate for simulating unsteady flow field in the transitional regime. The recent breakthroughs in high performance computing architecture in terms of speed and storage capacity have broken the computational bottleneck at very affordable prices and as a result Direct Numerical Simulation (DNS) and Large Eddy Simulation (LES) have come up as attractive techniques for investigating flow through LPT [15]-[24]. The predictive capability using DNS and LES approach based on high order numerical methods have improved to a great extent related to the flow problem where RANS models fail, and this led to decide the simulation strategies of three dimensional unsteady flow field.

In this study emphasis is put to predict the unsteady turbulence characteristics under flow separation and flow separation control conditions in experimental LPT cascade flow environment. Therefore, three dimensional unsteady numerical simulations under LPT flow conditions are carried out matching the experimental jet momentum coefficient and chord inlet Reynolds number. A High-Order LES turbulence model [25]-[28] developed by the author and tested by carrying out a detail study regarding its performance on various types of turbulent flow problem and DNS data is used. A detail study on eddy diffusive type LES model led to an understanding that an adequate mechanism to dissipate energy from resolved to sub-grid scales (SGS) is essential. The dynamic models have this property, but Smagorinsky model is too dissipative in laminar regions with mean shear and the correlation with the actual turbulent shear stress tensor is usually quite low. The excessive dissipation of the Smagorinsky model in laminar regimes is overcome if the model constant is replaced by a coefficient, which is dynamically obtained and depends on the local structure of the flow. In this case also the turbulent stress depends on the filter width, which depends on the grid width. In the present work, in a dynamic eddy viscosity model, a new approach is proposed to transfer information between the sub-grid and large scale eddies by solving an additional transport equation for turbulent kinetic energy in the grid scale level. Here, SGS turbulent stresses are closed using a dynamic turbulent kinetic energy transport model. The sub-grid scale length scale is represented by the minimum of the universal length scale and the grid scale. The universal length scale, which represents the blending of the length scales of cascade of eddies starting from the near wall small scale all the way to the sub-grid scale, is defined on the basis of turbulent Reynolds number in this model. A test filter was used for the dynamic procedure, which is applicable to stretched grid near the body surface. The advantages of such model include resolution of interesting scales, simultaneous modeling of high shear regions and large scale unsteadiness, and use of stretched grids. In the kinetic energy transport equation, dissipation of turbulent energy is defined on the basis of time scale. The transport equation for turbulent kinetic energy is solved in the sub-grid scale, by including the molecular diffusion of turbulent kinetic energy. The underpinning of the dynamic procedure employed here is the hypothesis corroborated by the experimental evidence, that

there is strong correlation between the SGS stress, and the sub-test scale Leonard's stress. The model parameter of dissipation term in the SGS turbulent kinetic energy equation is computed by a dynamic procedure based on the hypothesis that the dissipation rate of the resolved turbulent kinetic energy can be expressed in the same functional form as the dissipation rate of SGS kinetic energy. The present model has several desirable attributes that the Dynamic Smagorinsky Model (DSM) lacks. This model enjoys the benefits of a high-order turbulence model. Adopting SGS turbulent kinetic energy to parameterize the SGS stress renders this model better suited to non-equilibrium flows.

In LES, numerical diffusion however small it is, can easily overwhelm physical diffusion. Also, one of the problems encountered in LES of turbulent flow is the control of aliasing error. Use of schemes, which do not have a mechanism of controlling aliasing error can result in decay of the turbulence in a given flow field or an unbounded growth of the solution. In the present work, this problem is overcome by using a spatially high order accurate, upwind-biased WENO (Weighted Essentially Non-Oscillatory) [29] finite difference scheme developed for incompressible Navier-Stokes equations in three-dimensions. In our numerical method a fifth order upwind differencing technique is used for convective terms and fourth order central differencing technique is used for viscous diffusion terms. All these equations are solved using an efficient high order finite difference scheme of second order accuracy in time. A (H+O+H)-type patched grid approach preserving spatial accuracy in locally refined embedded region is used. Features of the flow-fields are described and compared with the experimental data on baseline case and active flow separation control case using VGJ. The results indicated that the active flow control could maintain attached flow over a longer distance compared to baseline case. And in turn could reduce the wake total pressure loss coefficient. The comparison of measured and computed results showed a good qualitative agreement, which led to the conclusion that in the present analysis the important features of the flow is successfully captured.

3   COMPUTATIONAL MODEL

In the present section turbulence model, basic equation, computation scheme, grid topology, and boundary conditions will be discussed.

3.1 TURBULENCE MODEL

Flow around turbine blades starts as laminar, but in most situations it inevitably becomes turbulent. Boundary layer transition from laminar to turbulent, which often cause a significant change in operational performance of the machinery, are generally influenced by the free-stream turbulence activity, existence of laminar separation bubble, and the pressure gradients. Therefore, accurate physics-based modeling of turbulence is very much important. Smagorinsky model is too dissipative in laminar regions with mean shear and the correlation with the actual turbulent shear stress tensor is usually quite low (about 0.3 in several flows). This eddy-diffusive type LES model has several shortcomings. The most problematic one, from practical standpoint, has to do with model constant, C_s. There is no single value of constant, which is universally applicable to a wide range of flows. The turbulent stress depends on the model constant C_s and the filter width, which in turn depends on the grid width. Therefore, excessive dissipation of Smagorinsky model in laminar regimes is overcome if the model constant is replaced by a coefficient, which is dynamically obtained and depends on the local structure of the flow. Another serious problem is that Smagorinsky model always gives a finite SGS viscosity even in

laminar region therefore it can not be used to simulate transitional flows, where the flow in question is laminar, either locally or intermittently.

In order to eliminate above mentioned physically unrealistic phenomena associated with the LES model, a High-Order LES turbulence model [25]-[28] is developed to physically satisfy the correct stream-wise blending between the pre-transitional pseudo-laminar boundary layer and the post-transitional fully turbulent boundary layer flow. In this regard a localized dynamic turbulent kinetic energy/time scale model is proposed to calculate the model constant dynamically. In this proposed model the SGS eddy viscosity is computed from

$$\nu_t = C_k k_{sgs}^{1/2} \overline{\Delta} \tag{1}$$

Consequently, SGS shear stress can be written as:

$$\tau_{ij} = -C_k k_{sgs}^{1/2} \overline{\Delta} \overline{S}_{ij} \tag{2}$$

k_{sgs} is obtained by solving its transport equation as:

$$\frac{\partial \overline{k}_{sgs}}{\partial t} + \frac{\partial \overline{u}_j \overline{k}_{sgs}}{\partial x_j} = -\tau_{ij} \frac{\partial u_i}{\partial x_j} - \frac{\overline{k}_{sgs}}{\overline{\tau}_{sgs}} + \frac{\partial}{\partial x_j} \left[\left(\frac{\nu_t}{\sigma_k} + \nu \right) \frac{\partial \overline{k}_{sgs}}{\partial x_j} \right] \tag{3}$$

The transport equation for turbulent kinetic energy is solved in the sub-grid scale, by including the molecular diffusion of turbulent kinetic energy. All the damping functions appeared in this transport equation are determined from the dynamic procedures. The underpinning of the dynamic procedure employed here is the hypothesis corroborated by the experimental evidence, that there is strong correlation between the sub-grid scale stress, τ_{ij}, and the sub-test scale Leonard's stress, L_{ij}. Using Germano's identity [30] as in Dynamic Smagorinsky Model (DSM), in the present model L_{ij} is defined as:

$$L_{ij} - \frac{\delta_{ij}}{3} L_{kk} = -2C_k \widetilde{\Delta} k_{tst}^{1/2} \widetilde{\overline{S}}_{ij} \tag{4}$$

Where, k_{tst} is the resolved turbulent kinetic energy associated with the scales between the test filter and grid filter. It can be directly computed from following equation.

$$k_{tst} = \frac{1}{2} \left(\widetilde{\overline{u_k u_k}} - \widetilde{\overline{u}}_k \widetilde{\overline{u}}_k \right) \tag{5}$$

The model parameter can then be obtained from Eqn.(4) by minimizing the error norm as in the DSM. Consequently, we have

$$C_k = \frac{\langle L_{ij} M_{ij} \rangle}{\langle M_{ij} M_{ij} \rangle} \tag{6}$$

with M_{ij} defined by

$$M_{ij} = -\widetilde{\Delta} k_{tst}^{1/2} \widetilde{\overline{S}}_{ij} \tag{7}$$

The dissipation rate of k_{tst} can also be computed from

$$\varepsilon_{tst} = (\nu + \nu_t) \left(\frac{\widetilde{\partial \overline{u}_i}}{\partial x_j} \frac{\widetilde{\partial \overline{u}_i}}{\partial x_j} - \frac{\partial \widetilde{\overline{u}}_i}{\partial x_j} \frac{\partial \widetilde{\overline{u}}_i}{\partial x_j} \right) \tag{8}$$

The present model has several desirable attributes that DSM lacks. First as a consequence of parameterizing L_{ij} directly, the dynamic procedure in the present model does not involve any test-filter operation on the model parameter, C_k. Thus, unlike the DSM, C_k is a genuine, local quantity free from any mathematical inconsistency. Secondly, C_k in this

model behaves numerically more benignly than C_k in the DSM, having much less fluctuation. Lastly this model enjoys the benefits of a high-order turbulence model. Adopting SGS turbulent kinetic energy to parameterize the SGS stress renders this model better suited to non-equilibrium flows. Alternatively stated, this method is extending the DSM to accurately model low frequency, large wavelength phenomena by utilizing LES approximations for the resolved unsteadiness.

Considering two length scales, one very near the wall, which is the Taylor micro-scale, and the other in the fully turbulent region (large scale energy containing eddies) following equation can be derived. The length scale for large scale eddies is defined as:

$$l_{dh} = \frac{C_d k^{1.5}}{\varepsilon} \tag{9}$$

However, near the wall, where the dissipation of turbulent kinetic energy is very large, the length scale is represented by the Taylor micro-scale defined as:

$$l_{dl} = C_{l1} \left(\frac{\nu k}{\varepsilon} \right)^{1/2}, \quad C_{l1} = \sqrt{2} \tag{10}$$

These two length scales can be related as:

$$\frac{l_{dh}}{l_{dl}} \propto R_{et}^{1/2}, \quad R_{et} = \frac{k^2}{\nu \varepsilon} \tag{11}$$

Eqn.(11) means that near the wall where, $R_{et} \to 0$, l_{dl} dominates the turbulence activity and away from the wall where R_{et} becomes very large, l_{dh} dominates. Thus R_{et} serves as a link between these two length scales of dissipation. The universal length scale l_u, which represents the blending of the length scales of cascade of eddies starting from the near wall small scale all the way to the sub-grid scale, is defined on the basis of R_{et} as follows;

$$l_u = C_u l_S R_{et}^{1/2}, \quad C_u = 0.65/\sqrt{2} \tag{12}$$

Where, l_S is near-wall smallest Taylor scale. In this model SGS time scale is defined as:

$$\overline{\tau}_{sgs} = \frac{\overline{k}_{sgs}}{\overline{\varepsilon}_{sgs}} \tag{13}$$

Where, $\overline{k}_{sgs}$ is obtained from Eqn.(3), and $\overline{\varepsilon}_{sgs}$ is obtained on the basis of following equation;

$$\overline{\varepsilon}_{sgs} = C_\varepsilon \frac{\overline{k}_{sgs}}{l_{sgs}} \tag{14}$$

The model parameter, C_ε in SGS dissipation rate of kinetic energy (Eqn.(14)) is also determined by a dynamic procedure using Eqn.(8).

$$C_\varepsilon = \frac{\widetilde{\Delta} \varepsilon_{tst}}{k_{tst}^{2/3}} \tag{15}$$

The SGS length scale l_{sgs} is represented by the minimum of l_u and C_k of Eqn.(1). This can be defined as follows;

$$l_{sgs} = \min(l_u, C_k \overline{\Delta}) \tag{16}$$

The SGS turbulent viscosity can be written as:

$$\nu_t = l_{sgs} k_{sgs}^{1/2} \tag{17}$$

3.2 NUMERICAL METHODLOGY

The basic equations are unsteady continuity and momentum equations for incompressible flows described by Eqn.(18) and Eqn. (19). A Poisson type equation for pressure derived from the momentum equations is solved to obtain the pressure field. The dependent variables including pressure have been non-dimensionalized by a characteristic velocity and length scale. All the equations are written in generalized coordinate to have sufficient grid resolutions in the near wall boundary layer region and generate grids to fit the body configuration. Accurate spatial discretization is crucial in LES. In LES, numerical diffusion however small it is, can easily overwhelm physical diffusion. It is something like measuring the frequency and amplitude of pressure oscillation of flow around test model using a wind tunnel having very high noise level. In this type of wind tunnel, even if you use a high response pressure transducer with very high accuracy, it is not possible to measure frequency of pressure oscillation accurately, because the wind tunnel noise level is so high that it will easily suppress the physical pressure oscillation phenomena. Also, one of the problems encountered in LES of turbulent flow is the control of aliasing error. Use of schemes, which do not have a mechanism of controlling aliasing error can result in decay of the turbulence in a given flow field or an unbounded growth of the solution. In the present work, this problem is overcome by using a spatially high order accurate, upwind-biased WENO [29] finite difference scheme developed for incompressible Navier-Stokes equations. In the present method a fifth order upwind differencing technique is used for convective terms and fourth order central differencing technique is used for viscous diffusion terms. All these equations are solved using an efficient high order finite difference scheme of second order accuracy in time. In this approach, fully implicit finite difference equations are solved performing several iterations at each time step to make the differencing errors zero.

$$\nabla \cdot \boldsymbol{u} = 0 \tag{18}$$

$$\frac{\partial \boldsymbol{u}}{\partial t} + \boldsymbol{u} \nabla \cdot \boldsymbol{u} = -\nabla p + \frac{1}{\mathrm{Re}} \nabla^2 \boldsymbol{u} \tag{19}$$

3.3 GRID TOPOLOGY AND BOUNDARY CONDITIONS

Sondergaard et al. performed experiment using a linear cascade of turbine blades. The axial chord length and the span of the blades were 0.089 m and 0.088 m, respectively. Solidity, defined as the axial chord to spacing ratio of 0.75 was used. The inlet flow angle α_i and the design exit flow angle α_0 were chosen as 35 deg. and 60 deg., respectively. Schematic of the LPT blade shape is presented in Figure 1. The turbine blade used in their experiment was a research design "PakB" provided by the Pratt & Whitney. The blade geometries correspond to a typical Mach number scale version highly-loaded LPT. Where, c, s and q_i are turbine blade axial chord, non-dimensional span-wise domain extent and non-dimensional inlet planar velocity magnitude, respectively. The purpose of their experiment was to investigate the acts of VGJ on mitigating the effects of separation on the blade suction surface and in turn controlling the flow separation. Air was injected through holes drilled in the blade suction surface at a pitch angle of 30 deg. and a skew angle of 90 deg. to generate the jets. Here the angle the jet makes with local surface is defined as pitch, and the angle of projection of the jet on the surface, relative to the local free-stream direction is defined as the skew. The size of the drill used to develop the holes is defined as the jet diameter. In the experiment jet diameter of 0.001 m was used. Due to the orientation, the jet exit shape is elliptic and the jet exit velocity vector comprised of the blade-normal and span-wise components. The computational domain surrounding the blade was described by a body fitted grid topology to satisfy proper grid resolution near the body surface, whose origin was located at the inboard leading edge of the blade. The mesh employs an (H+O+H)-type patched grid topology to discretize the regions surrounding the experimental LPT cascade. The airfoil geometry used in the current study is the same as that used in the experimental investigation of Sondergaard et al.. The geometry consists of the LPT blade with three VGJ holes.
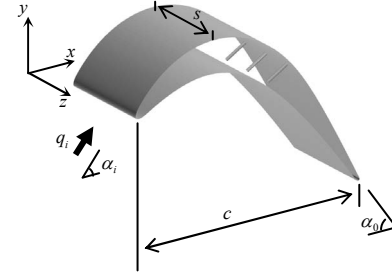

Figure 1. Turbine blade configuration

The computational grid about the turbine blade is presented in Figure 2. In Figure 2(a), (b) and (c) show x-y plane, blade surface and magnified view including the holes, respectively. In the case of O-type grid topology, along the circumferential, blade normal and span-wise directions, 491, 189 and 101 points, respectively were used. Minimum spacing in the normal direction at the blade surface corresponds to y^+ less than 0.1. To properly capture the correct physical behavior associated with the unsteady flow for the flow control case, grid resolution in the jet and jet wake region in enhanced. This was done by embedding refined mesh in this region. A series of patch grid topology was used to describe the elliptic jet geometry. Zones upstream and downstream the blade is used to extend the inlet and outlet region of the blade cascade. The multi-zone grid used to describe the region consisted of 6 zones. Three zonal grids for three VGJ holes (H-type) and one zonal grid each for the blade upstream, downstream (H-type) and the blade configuration (O-type) are used. The jet nozzle interior to the blade can be seen in Figure 2(c). This was extended a distance of four jet diameters below the surface and was included in the simulations. A non-uniform span-wise mesh distribution was utilized with grid points clustering near the jet exit. Although the actual grids used for the calculations are very dense near the airfoil surfaces (to resolve the viscous effects), for the purpose of clarity Figure 2 shows grids in which some points are omitted in all the three directions.

Inflow and outflow conditions for the complete turbine blade cascade domain used in the simulation were specified in a manner consistent with subsonic internal flows. Along the upstream boundary, the inlet flow velocity obtained from the experimental Reynolds number and inlet flow angle were specified, and the inlet static pressure was obtained through extrapolation from the interior solution. The downstream boundary of the computation domain is subsonic exit boundary. An implicit extrapolation procedure to obtain variables other than pressure was used at this boundary. The implicit extrapolation is followed by a post-update correction wherein the exit static pressure is specified. Generally specifying static pressure at the exit boundary reflects the pressure waves that reach the exit boundary back into the system. In order to avoid this reflective property at the exit boundary, an alternative exit boundary condition is used in this study. This is a partially non-reflective procedure developed by Erdos [31]. This boundary condition is non-reflective for waves or components of waves that are perpendicular to the exit boundary (pressure variations in the

flow direction only) and is reflective for waves that are parallel to the exit boundary (pressure variation in the flow normal direction only). There are several boundaries that are used in the present calculation. These boundaries serve to connect various zones. The zonal boundary conditions must meet certain requirements before they can be used effectively. At the interface boundary between upstream and blade, the blade and downstream zone, and the holes and the blade surface an implicit flux conservation technique is used to pass the information between the two zones. At the wall boundaries, which correspond to airfoil surface and the walls of jet nozzles no-slip condition for velocity is specified. In the case of pressure the derivative of pressure with respect to the normal distance from the wall surface is set to zero. Periodic boundary conditions were used in the blade pitch-wise direction.
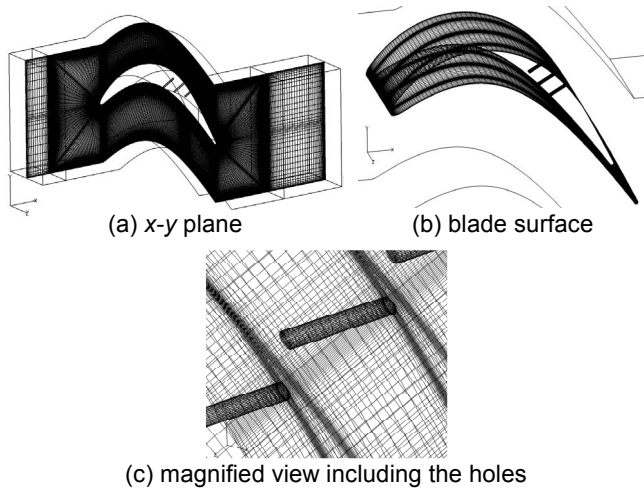

(a) x-y plane   (b) blade surface

(c) magnified view including the holes

Figure 2. Computational grid

4   RESULTS AND DISCUSSION

Computations for baseline case of LPT cascade flow for two different Reynolds number (5.0×10^4, 1.0×10^5) and the flow control using steady VGJ was carried out using a High-Order LES approach for turbulence modeling. To properly demonstrate the usefulness of VGJ for boundary layer separation control, the flow separation must first be documented for the uncontrolled case, before proceeding with the results of the application of control. Here some typical results on the baseline performance for two different flow-Reynolds number conditions without blowing and the effects of steady vortex generator jets on flow separation control will be discussed in section 4.1 and section 4.2, respectively.

4.1 BASELINE CASE (WITHOUT VGJ)

In Figure 3 and Figure 4 are presented the measured and computed time-averaged and span-wise spatially averaged surface pressure coefficient along the axial chord of the blade for the uncontrolled case (without VGJ) under flow-Reynolds number of 5.0×10^4 and 1.0×10^5, respectively. The horizontal and vertical axis represent non-dimensional chord length and pressure coefficient, respectively. The line represents the computed results and the symbols represent the experimental results [1]. In Figure 3, the flattened region or plateau in the surface pressure coefficient distribution under lower flow-Reynolds number (5.0×10^4) baseline conditions represent the characteristic of massively separated flow between 65% to 90% axial chord on the suction surface. The computed results predicted the

separation region quite satisfactorily. The results on velocity and vorticity distribution on the blade surface will help to have a better understanding of this flow separation phenomenon. In Figure 4, it can be observed that the flattened region or plateau in the surface pressure coefficient distribution under higher flow-Reynolds number (1.0×10^5) baseline conditions represent the characteristic of separated flow occurs only to a limited portion of the axial chord (between 80% to 85%) on the suction surface and in the further downstream there occurs an abrupt drop in pressure coefficient (representing flow reattachment in that region). The comparison of Figure 3 and Figure 4 leads to an understanding that the extent of the flow separation region increases with decreasing Reynolds number. This difference in flow separation characteristic with the change in Reynolds number could also be clearly observed from the results related to time-averaged and span-wise spatially averaged velocity and vorticity distribution that will be presented later. The computed results predicted the experimentally observed flow separation behavior quite satisfactorily.
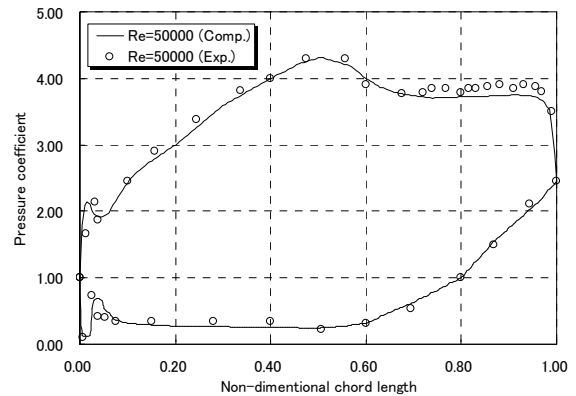

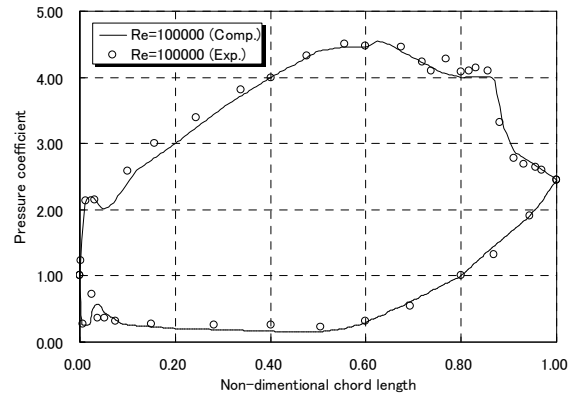**Figure 3.** Surface pressure coefficient distribution (Re=5.0×10^4)

Figure 4. Surface pressure coefficient distribution (Re=1.0×10^5)

In the experiment, to document this region of interest, boundary layer traverses were made using sub-miniature hot film probe at 67%, 73% and 79% axial chord on the blade suction surface for both the flow-Reynolds number condition. In Figure 5 and Figure 6 are presented the measured and computed time-averaged and span-wise spatially averaged axial velocity boundary layer profiles at three different axial chord locations on the suction surface under flow-Reynolds number of 5.0×10^4 and 1.0×10^5, respectively. The horizontal and vertical axis represent the non-dimensional velocity with respect to

the mid-channel velocity and wall normal distance in cm, respectively. Here also, the line represents the computed results and the symbols represent the experimental results [1]. In the experiment, each point in the profile represented 40,000 data points taken at 10 kHz. In Figure 5, at the location of 67% axial chord the boundary layer axial velocity profile is attached but highly unsteady. At the location of 73% and 79% axial chord the axial velocity profile is obviously separated with velocities in the separated region approaching zero. The region of separation is extended towards the axial chord downstream locations. In the experiments, time-resolved hot film traces taken at near-wall region for 73% axial chord location showed a wide velocity of fluctuations in the separated region and the shear layer respectively. The results presented in Figure 9 and Figure 10 on the instantaneous axial velocity, normal velocity, and vorticity distributions for two different flow-Reynolds number conditions will lead to have a good understanding regarding the above mentioned experimentally observed unsteady near wall flow behavior. The results presented in Figure 6 indicated that the axial velocity boundary layer profile at these axial chord locations on the suction surface are well-behaved laminar or transitional flow at least up to 79% of suction surface axial chord locations.
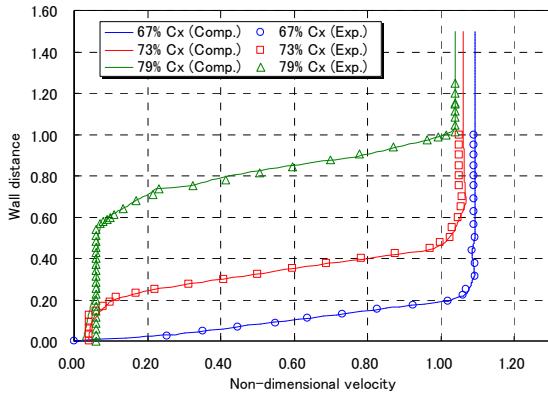
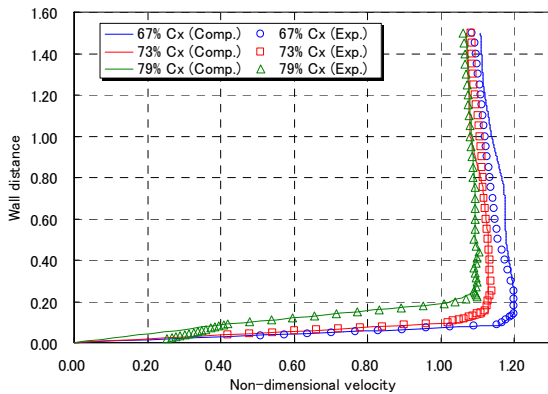**Figure 5.** Boundary layer profiles of streamwise velocity (Re=5.0x10^4)

Figure 6. Boundary layer profiles of streamwise velocity (Re=1.0x10^5)

In Figure 7(a),(b) and Figure 8(a),(b) are presented time-averaged axial velocity and vorticity distribution in the mid-span plane for flow-Reynolds number of 5.0x10^4 and 1.0x10^5, respectively. In these figures, red color represents maximum positive value and blue color represents

the minimum negative value. The results presented in Figure 7 and Figure 8 justified the results of the experimentally observed flow behavior (the extent of the separation region increases with decreasing Reynolds number) presented in Figure 3-Figure 6, that in the case of lower flow-Reynolds number conditions (5.0x10^4), flow separation starts from about 60% of axial chord on the suction surface and gets extended all the way downstream, however, in the case of higher flow-Reynolds number condition (1.0x10^5) flow separation starts from about 80% of axial chord on the suction surface and gets reattached at about 5% downstream the separation location.
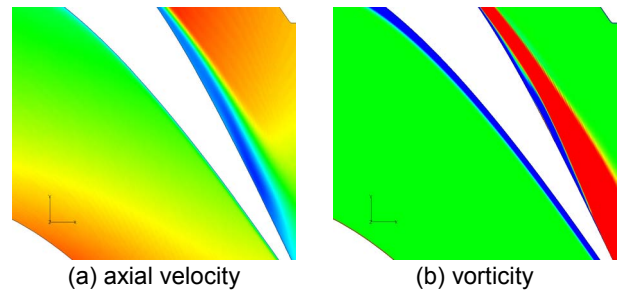
(a) axial velocity   (b) vorticity

Figure 7. Time -averaged distribution (Re=5.0x10^4)
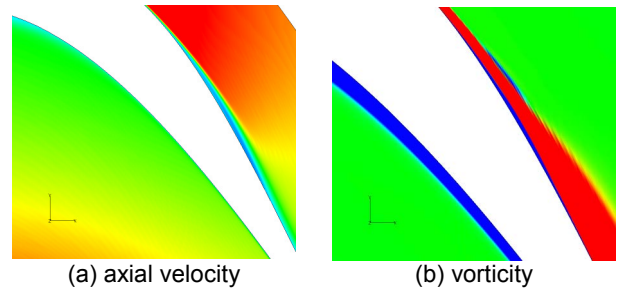
(a) axial velocity   (b) vorticity

Figure 8. Time-averaged distribution (Re=1.0x10^5)

In Figure 9(a)-(c) and Figure 10(a)-(c) are presented three dimensional representations of the flow depicted by iso-surfaces of the instantaneous axial velocity, normal velocity, and vorticity for flow-Reynolds number of 5.0x10^4 and 1.0x10^5, respectively. In all these figures, contour represents pressure distribution, and red color represents maximum positive value and blue color represents the minimum negative value. The results presented here helped to have a good understanding of how the flow instability that occurs just upstream the separation location sustains with the aid of the adverse pressure gradient effect (Re=5.0x10^4) and the region of instability grew in the downstream region due to strong turbulence activity, results from wide velocity fluctuations in the separated region and the near wall shear layer (Figure 9). On the other hand, in the case of higher flow-Reynolds number the instability that occur just upstream the separation location is not sustained (the turbulence activity in flow separation and wall-near shear layer region is weak due to low velocity fluctuations), get dissipated away downstream and the flow reattached again in the downstream region (Figure 10). These figures show unsteady structure in the separated flow regions. These structures are more easily discerned in instantaneous vorticity iso-surface appearing in Figure 9(c) and Figure 10(c). Figure 9(c) shows that extensive unsteady separated flow region has a richer content of small scale structures due to break down and transition to a more complex situation. Results on rms pressure that are not presented here, indicated that the location of reattachment downstream the separation region is associated with a flow stagnation region and the peak of the rms pressure exists near the

stagnation region where the flow gets reattached (higher flow-Reynolds number conditions). In the case of lower flow-Reynolds number condition, since the flow separates away from the wall no stagnation region (occur due to reattachment of flow) can be observed.
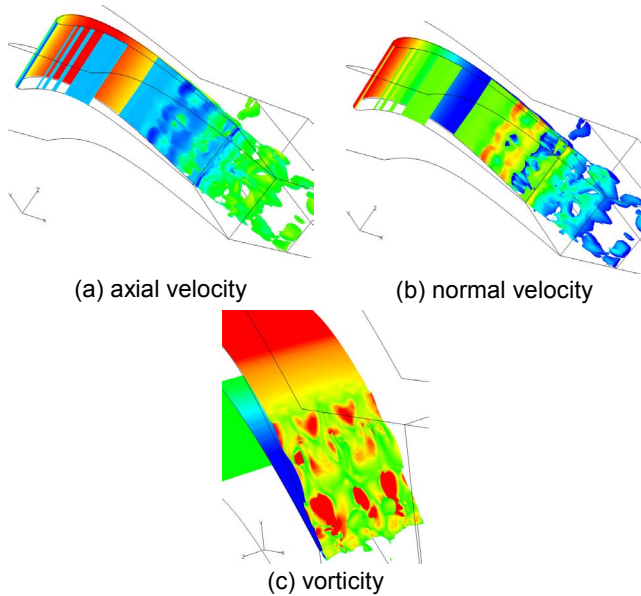

(a) axial velocity
(b) normal velocity

(c) vorticity

Figure 9. Instantaneous iso-surface (Re=5.0x10^4)

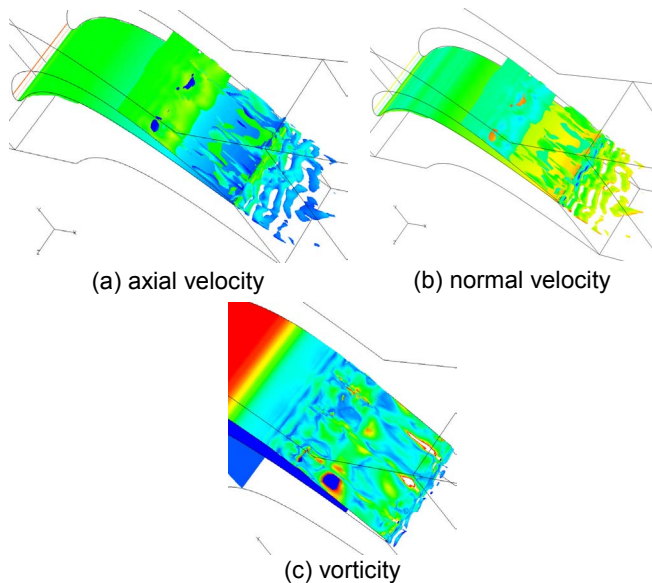(a) axial velocity
(b) normal velocity

(c) vorticity

Figure 10. Instantaneous iso-surface (Re=1.0x10^5)

4.2 SEPARATION CONTROL CASE (WITH VGJ)

Experimental investigations of flow separation control by the VGJ used the jet blowing ratio (the ratio of jet exit velocity magnitude to the local free-stream velocity) as a parameter to describe characteristics of VGJ. In the present study, three VGJ (having blowing ratio of 2.0) are used for the lower flow-Reynolds number (5.0x10^4) case. In Figure 11(a)-(c) are presented the results on instantaneous axial velocity, normal velocity, and vorticity distribution at the mid-hole (mid-span) plane. In all these figures, red color represents maximum positive value and blue color represents the minimum negative value. It can be observed here that the flow control maintains attached flow and decreases the vertical extent of the wake relative to the baseline case. Unsteady structures are visible in separated flow regions and these structures are more easily discerned in instantaneous vorticity distribution shown in Figure 11(c). The results indicate that in this case, the fundamental effect of flow control was to energize the blade boundary layer due to transfer of fluid momentum and mixing of the jet with the main flow near the wall-near boundary layer. This helped maintain attached flow along the blade surface for a distance greater than that of the baseline case. As a result, wake total pressure losses were decreased appreciably.
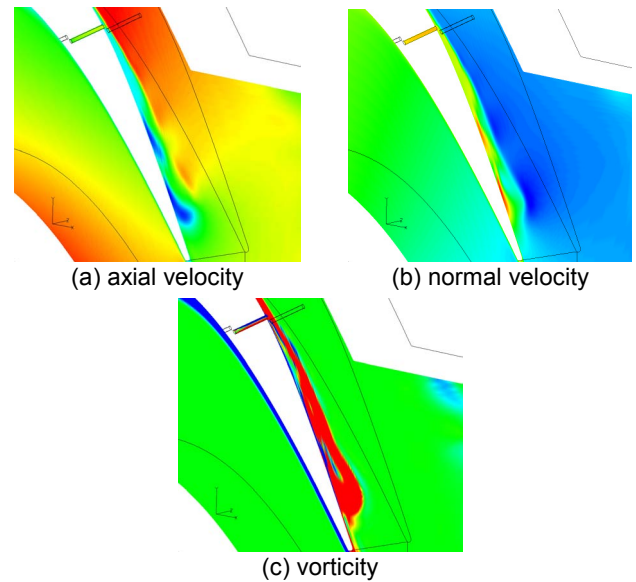

(a) axial velocity
(b) normal velocity

(c) vorticity

Figure 11. Instantaneous distribution (Re=5.0x10^4)

In Figure 12(a)-(c) are presented three dimensional representations of the flow depicted by the iso-surfaces on instantaneous axial velocity, normal velocity, and vorticity iso-surface for VGJ flow control case. In all these figures, contour represents pressure distribution, and red color represents maximum positive value and blue color represents the minimum negative value. It is seen here that in this case vorticity is being generated in the boundary layer in close proximity to the blade surface. When the boundary layers separate in these situations, it is much less dramatic than in the uncontrolled case. The value of iso-surfaces corresponds approximately to that at the edge of the shear layer upstream of separation. Both the vertical and span-wise extent of the turbulent structures is visible here. Iso-surfaces of span-wise vorticity in the near jet region, as viewed downstream of the jet, are provided in Figure 12(c). In this case, unsteadiness can be observed in the jet surface, just downstream of the nozzle exit. The results indicated that the wake of the jet extends across the span-wise domain. The results presented here showed that the jet penetrates to a height greater than the boundary layer thickness and mixing persists downstream. Because of the orientation of the jet transverse to the stream-wise flow (blade-normal and span-wise), it is fundamentally unstable and rapidly evolves to a non-coherent form. The process serves to generate mixing between jet and main flow in the separation region.
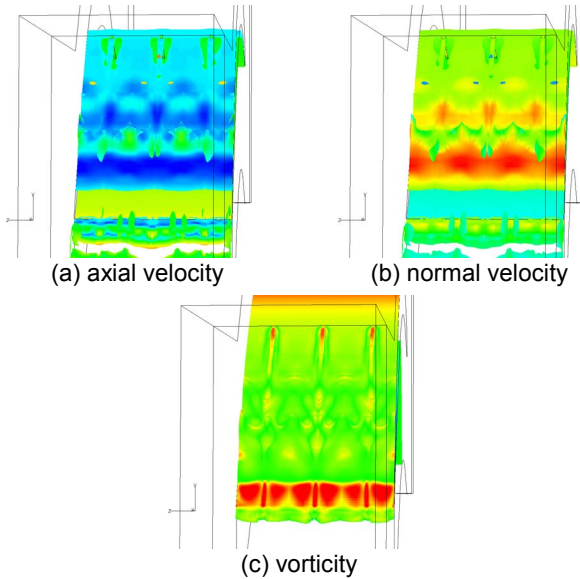
Copyright © 2010 by ASME

(a) axial velocity   (b) normal velocity

(c) vorticity

Figure 12. Instantaneous iso-surface (Re=5.0x10⁴)

5   CONCLUDING REMARKS

Three dimensional incompressible unsteady viscous flow analysis was carried out to describe the transitional subsonic flow through a highly loaded LPT under two different flow-Reynolds number conditions (baseline case) and with steady VGJ to control separation for lower Reynolds number case using a High-Order LES approach to model unsteady turbulence characteristics. The computation method used patched grids to simulate the LPT cascade including three VGJ nozzles. The integration method was a WENO type upwind scheme which is spatially fifth order accurate and temporally second order accurate. Upwind finite difference scheme is set in an iterative implicit framework. The results are expected to be used to great advantage in understanding unsteady flow separation behavior in highly loaded LPT under low flow-Reynolds number conditions and its subsequent control.

Comparisons were made between the measured and time-averaged and span-wise spatially averaged results on surface pressure coefficient distribution along axial chord and axial velocity profile for two different flow-Reynolds number conditions (baseline case) without using VGJ. Experimentally observed physical behavior of massively flow separation region on the blade suction surface downstream region for lower flow-Reynolds number conditions and the increase in extent of the separation region with decreasing Reynolds number is very well predicted. The separated axial velocity boundary layer profile (Re=5.0x10⁴) in the downstream region and the occurrence of well-behaved laminar or transitional flow profile at all the measured locations (Re=1.0x10⁵) is also well predicted. Instantaneous velocity and vorticity iso-surface results helped to have a good understanding of how the flow instability that occurs just upstream the separation location sustains by the pressure gradient effect (Re=5.0x10⁴) and the region of instability grew in the downstream region due to strong turbulence activity results from wide velocity fluctuations in the separated region and the near wall shear layer. This turbulence characteristic results in the flow to separate away from the wall. On the other hand, in the case of higher flow-Reynolds number the instability that occur just upstream the separation location get dissipated away downstream and the flow reattached again in the downstream region.

The increase in flow-Reynolds number led to a reduction in the size of separation zone. This was also evident from the results of dramatic reduction in wake momentum deficit with increasing Reynolds number.

In the case of steady VGJ, the fundamental effect of flow control was to energize the blade boundary layer due to transfer of fluid momentum and mixing of the jet with the main flow near the wall-near boundary layer. This helped maintain attached flow along the blade surface for a distance greater than that of the baseline case. As a result, wake total pressure losses were decreased appreciably. The results of this study led to an understanding that our physics-based turbulence model associated with the numerical method could predict the experimentally observed physical phenomena quite satisfactorily.

Finally, CPU time required for the present computation is about 24 hours using NEC SX9 Vector Computer (single CPU). However, it's not possible to compare the CPU time required for LES to that of RANS type model. Because grid resolution and other factors matter for the CPU time of RANS type model.

REFERENCES

[1] R.Sondergaard, R.B.Rivir and J.P.Bons, 2002, Control of Low Pressure Turbine Separation Using Vortex Generator Jet, *Journal of Propulsion and Power*, 18-4, pp.889-895.

[2] R.V.Chima, 1985, Inviscid and Viscous Flows in Cascades with an Explicit Multiple-Grid Algorithm, *AIAA Journal*, 23-10, pp.1556-1563.

[3] R.V.Chima, 1987, Explicit Multiple-Grid Algorithm for Quasi-Three-Dimensional Viscous Flows in Turbo-machinery, *Journal of Propulsion and Power*, 3-5, pp.397-405.

[4] W.N.Dawes, 1987, A Numerical Analysis of the Three-Dimensional Viscous Flow in a Transonic Compressor Rotor and Comparison with experiment, *ASME Journal of Turbomachinery*, 109-1, pp.83-90.

[5] R.L.Davis, R.H.Ni., and J.E.Carter, 1987, Cascade Viscous Flow Analysis Using the Navier-Stokes Equations, *Journal of Propulsion and Power*, 3-5, pp.406-414.

[6] K.F.Weber, D.W.Thoe., and R.A.Delaney, 1990, Analysis of Three-Dimensional Turbomachinery Flows on C-type Grids Using an Implicit Euler Solver, *ASME Journal of Turbomachinery*, 12, pp.362-369.

[7] Y. Yamamoto, H. Daiguji, and H. Ishigaki, 1988, An Implicit Time-Marching Scheme for Solving the Compressible Navier-Stokes Equations, Computational Fluid Dynamics, G.D.V. Davis, and C.Fletcher, eds., *Elsevier Science Publishers B.V.*, North-Holland.

[8] B.C.Weinberg, R.J.Yang, H. Mcdonald, and S.J.Shamroth, 1986, Calculation of Two- and Three-dimensional Transonic Cascade Flow Fields Using the Navier-Stokes Equations, *ASME Journal of Engineering for Gas Turbine and Power*, 108, pp.93-102.

[9] C.Hah, 1989, Numerical Study of Three-Dimensional Flow and Heat Transfer Near the Endwall of Turbine Blade Row, *AIAA Paper*, 89-1689.

[10] F.Eulitz and K.Engel, 1998, Numerical Investigation of Wake Interaction in a Low Pressure Turbine, *ASME Paper*, 98-GT-563.

[11] C.H.Choi and J.Y.Yoo, 1998, Cascade Flow Calculations Using the k-ω Turbulence Model with Explicit-Implicit Solver, *AIAA Journal*, 35-9, pp.1551-1552.

[12] A.Chernobrovkin and B.Lakshminarayana, 1999, Turbulence Modeling and Computation of Viscous Transitional Flows for Low Pressure Turbines, *Journal of Fluid Engineering*, 121-4, pp.824-833.

[13] D.J.Dorney, D.E.Ashpis, D.E.Halstead and D.C.Wisler, 2000,

Study of Boundary-Layer Development in a Two-Stage Low-Pressure Turbines, *Journal of Propulsion and Power*, 16-1, pp.160-163.

[14] Y.B.Suzen, P.G.Huang, L.S.Hultgren and D.E.Ashpis, 2001, Predictions of Separated and Transitional Boundary Layers Under Low-Pressure Turbine Airfoil Condition using an Intermittency Transport Equation, *AIAA Paper*, 2001-0446.

[15] B.Raverdy, I.Mary, P.Sagaut and N.Liamis, 2001, Large-Eddy Simulation of the Flow Around a Low Pressure Turbine Blade, *Direct and Large-Eddy Simulation IV*, 8, pp.381-388.

[16] R.Mittal, S.Venkatasubramanian and F.M.Najjar, 2001, Large-Eddy Simulation of Flow Though a Low-Pressure Turbine Cascade, *AIAA Paper*, 2001-25560.

[17] D.Postl, A.Gross and H.F.Fasel, 2003, Numerical Investigation of Low-Pressure Turbine Blade Separation Control, *AIAA Paper*, 2003-0614.

[18] D.P.Rizzetta and M.R.Visbal, 2003, Numerical Investigation of Transitional Flow Through a Low-Pressure Turbine Cascade, *AIAA Paper*, 2003-3587.

[19] JG.Wissink, 2003, DNS of Separating, Low-Reynolds Number Flow in a Turbine Cascade with Incoming wakes, *International Journal of Heat and Fluid Flow*, 24-4, pp.626-635.

[20] G.Kalitzin, X.Wu and P.A.Durbin, 2003, DNS of Fully Turbulent Flow in a LPT Passage, *International Journal of Heat and Fluid Flow*, 24-4, pp636-644.

[21] D.Postl, A.Gross and H.F.Fasel, 2004, Numerical Investigation of Active Flow Control for Low-Pressure Turbine Blade Separation, *AIAA Paper*, 2004-750.

[22] D.P.Rizzetta and M.R.Visbal, 2004, Numerical Simulation of Separation Control for a Highly-Loaded Low-PressureTurbine, *AIAA Paper*, 2004-2204.

[23] A.Gross and H.F.Fasel, 2004, Active Control of Separation for Low-Pressure Turbine Blade, *AIAA Paper*, 2004-2203.

[24] D.P.Rizzetta and M.R.Visbal, 2005, Numerical Study of Active Flow Control for a Transional Highly-Loaded Low-Pressure Turbine, *AIAA Paper*, 2005-5020.

[25] D.Biswas et al., 2002, Application of a Two-equation Low-Reynolds Number Version Turbulent Model to Transitional Boundary Flows, *AIAA Paper*, 2002-2748.

[26] D.Biswas et al., 1994, Calculation of Transitional Boundary Layers with an Improved Low-Reynolds Number Version k-ε Turbulence model, *ASME Journal of Turbomachinery*, 116, pp.765-773.

[27] D.Biswas, 2006, Studies on Separation Control CFD Validation Test Case Based on a Higher Order LES Model, *AIAA Paper*, 2006-2881.

[28] D.Biswas, 2006, Studies on Unsteady Laminar-Turbulent Transition in a Low Pressure Turbine Flow Based on a Higher Order LES model, *AIAA Paper*, 2006-3684.

[29] Chi-Wang Shu, 1997, Essentially Non-Oscillatory and Weighted Essentially Non-Oscillatory Schemes for Hyperbolic Conservation Laws, *ICASE Report*, 97-65.

[30] M.Germono, U.Piomelli, P.Moin, W.H.Cabot, 1991, A Dynamic Subgrid-scale Eddy Viscosity Model, *Phys. Fluid*, A3-7, pp.1760-1765.

[31] J.I.Erdos, E.Alzner and W.McNally, 1977, Numerical Solution of Periodic Transonic Flow Through a Fan Stage, *AIAA Journal*, 15-11, pp.1559-1568.